Astronomy & Astrophysics

LETTER TO THE EDITOR

Apparent superluminal core expansion and limb brightening in the candidate neutrino blazar TXS 0506+056

E. Ros[1], M. Kadler[2], M. Perucho[3,4], B. Boccardi[1], H.-M. Cao[5], M. Giroletti[5], F. Krauß[6], and R. Ojha[7,8,9]

[1] Max-Planck-Institut für Radioastronomie, Auf dem Hügel 69, 53121 Bonn, Germany
   e-mail: ros@mpifr-bonn.mpg.de
[2] Lehrstuhl für Astronomie, Universität Würzburg, Emil-Fischer-Straße 31, 97074 Würzburg, Germany
[3] Departament d'Astronomia i Astrofísica, Universitat de València, c/ Dr. Moliner 50, 46100 Burjassot, València, Spain
[4] Observatori Astronòmic, Universitat de València, c/ Catedràtic José Beltrán Martínez 2, 46980 Paterna, València, Spain
[5] INAF – Istituto di Radioastronomia, Via Gobetti 101, 40129 Bologna, Italy
[6] Department of Astronomy and Astrophysics, Pennsylvania State University, University Park, PA 16801, USA
[7] National Aeronautics and Space Administration/Goddard Space Flight Center, Greenbelt, MD 20771, USA
[8] University of Maryland, Baltimore County, 1000 Hilltop Cir, Baltimore, MD 21250, USA
[9] Catholic University of America, Washington, DC 20064, USA

ABSTRACT

Context. IceCube has reported a very-high-energy neutrino (IceCube-170922A) in a region containing the blazar TXS 0506+056. Correlated gamma-ray activity has led to the first high-probability association of a high-energy neutrino with an extragalactic source. This blazar has been found to be in a radio outburst during the neutrino event.
Aims. Our goal is to probe the sub-milliarcsecond properties of the radio jet right after the neutrino detection and during the further evolution of the radio outburst.
Methods. We performed target of opportunity observations at 43 GHz frequency using very long baseline interferometry imaging, corresponding to 7 mm in wavelength, with the Very Long Baseline Array two and eight months after the neutrino event.
Results. We produced two images of the radio jet of TXS 0506+056 at 43 GHz with angular resolutions of (0.2×1.1) mas and (0.2×0.5) mas, respectively. The source shows a compact, high brightness temperature core, albeit not approaching the equipartition limit and a bright and originally very collimated inner jet. Beyond approximately 0.5 mas from the millimeter-VLBI core, the jet loses this tight collimation and expands rapidly. During the months after the neutrino event associated with this source, the overall flux density is rising. This flux density increase happens solely within the core. Notably, the core expands in size with apparent superluminal velocity during these six months so that the brightness temperature drops by a factor of three despite the strong flux density increase.
Conclusions. The radio jet of TXS 0506+056 shows strong signs of deceleration and/or a spine-sheath structure within the inner 1 mas, corresponding to about 70–140 pc in deprojected distance, from the millimeter-VLBI core. This structure is consistent with theoretical models that attribute the neutrino and gamma-ray production in TXS 0506+056 to interactions of electrons and protons in the highly relativistic jet spine with external photons originating from a slower moving jet region. Proton loading due to jet-star interactions in the inner host galaxy is suggested as the possible cause of deceleration.

Key words. radiation mechanisms: non-thermal – neutrinos – techniques: interferometric – radio continuum: galaxies – quasars: individual: TXS 0506+056

1. Introduction

On September 22, 2017, the IceCube Neutrino Observatory (IceCube Collaboration 2017) detected a ~290 TeV neutrino (IceCube-170922A) from a direction consistent with the flaring γ-ray, radio-loud blazar TXS 0506+056, with a positional uncertainty of 0.4–0.8° (IceCube Collaboration 2018a), resulting in a ~3σ significance of an association. In addition, the IceCube Collaboration (2018b) report a ~3.5σ excess of 13 ± 5 neutrino events in the direction of TXS 0506+056 during a six-month period in 2014–2015 without accompanying bright γ-ray flaring. These two observations diverge in that Reimer et al. (2019) and Rodrigues et al. (2019) find that single-zone models cannot explain the spectral energy distribution (SED) during the γ-ray faint 2014–2015 period.

TXS 0506+056 has a redshift of 0.3365 ± 0.0010. This corresponds to a luminosity distance of 1762 Mpc. An angular distance of 1 mas in the sky corresponds to a linear scale of 4.78 pc[1]. This source is classified as a BL Lac object, although Padovani et al. (2019) present arguments for a quasar-like nature for this source.

An intensive multiwavelength campaign followed the Ice-Cube detection, covering the whole electromagnetic spectrum; see IceCube Collaboration (2018a). These observations resulted in the first redshift measurement (Paiano et al. 2018) and the detection of TXS 0506+056 at teraelectronvolt energies by the MAGIC telescopes (Ansoldi et al. 2018). In the radio band, the Owens Valley Radio Observatory has been monitoring this

---

[1] We use $H_0 = 71\,\mathrm{km\,s^{-1}\,Mpc^{-1}}$, $\Omega_\Lambda = 0.73$ and $\Omega_\mathrm{m} = 0.27$.
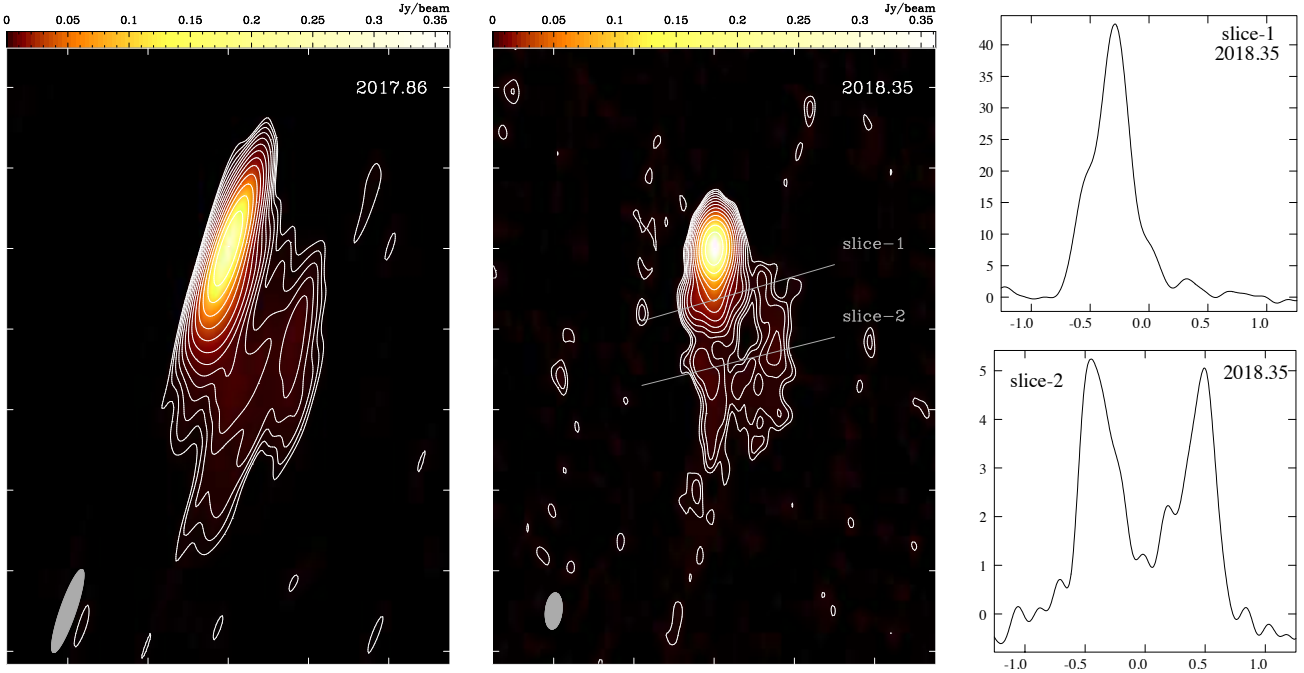
Fig. 1. Forty-three GHz VLBA images of TXS 0506+056 on Nov 11, 2017 (*left panel*), and May 4, 2018 (*middle panel*). Apart from the different beam sizes, the resolved structure is not significantly different. Image parameters are given in Table 1. The distance between the ticks on the axes is 1 mas, corresponding to 4.78 pc at the distance of TXS 0506+056. *Right panels*: surface brightness profiles (mJy beam^{-1} vs. mas, relative to the slice mid-point) for two slices transverse to the jet, as shown in the *middle panel*.

source over the last ten years at 15 GHz (Richards et al. 2011) and has registered an increase in the flux density since early 2017[2]. The MOJAVE program (Monitoring of Jets in Active Galactic Nuclei with VLBA Experiments, Lister et al. (2009, 2018) is also monitoring this source with 15 GHz very long baseline interferometry (VLBI) imaging since 2009[3]. The MOJAVE collaboration reports maximum jet speeds of $0.98 \pm 0.31c$ (Lister et al. 2019), which is a relatively low apparent jet speed compared to the overall speed distribution in the MOJAVE program. Such low jet velocities, however, are frequently reported for a number of BL Lac objects emitting tera electron volts (e.g., Piner & Edwards 2014, 2018, and references therein).

Based on public archival MOJAVE data, Kun et al. (2018) report that the increase in flux density observed can be assigned to the most central region of the source, associated with the 2 cm core of the parsec-scale image (i.e., with the inner ~1 mas). Another publication making use of the public MOJAVE database (Britzen et al. 2019) claims the possible presence of a second jet in TXS 0506+056, which might interact with the primary jet giving rise to enhanced neutrino emission. Higher frequency VLBI observations provide increased angular resolution and allow us to peer deeper into the VLBI core where the radio variability originates. These observations also allow us to test for the presence of a possible secondary jet core and for signs of a jet–jet interaction as proposed by Britzen et al. (2019). Moreover, high-resolution VLBI observations can probe the internal jet structure and test the existence of velocity gradients, either along the jet axis (jet acceleration/deceleration) or perpendicular to it (spine-sheath structure). Such gradients might play a crucial role in the γ-ray emission and correlated neutrino production, as proposed by several authors in relation to TXS 0506+056 (Tavecchio et al. 2014; Righi et al. 2017; Ansoldi et al. 2018;

---

[2] See the corresponding light curve at their webpage.
[3] See the imaging database at the MOJAVE webpage.

Table 1. VLBA observational journal experiments (BR224).

Date YYYY-MM-DD	Freq. [GHz]	43 GHz beam [μas × μas]	[°]	S_{tot} [mJy]	S_{peak} [mJy beam^{-1}]	S_{min} [mJy beam^{-1}]
2017-11-10 [a]	15/23/43/86	1090 × 195	−19	496	320	0.63
2018-05-04	43/86	451 × 207	−7	719	403	0.73

Notes. [a]Brewster and Saint Croix did not participate in this epoch.

Zhang et al. 2019). We present millimeter-VLBI observations of TXS 0506+056 during the radio outburst associated with the IceCube-170922A neutrino event.

2. Observations and data reduction

We observed TXS 0506+056 using the VLBA as soon as possible after the IceCube detection. At that time, the easternmost station, Saint Croix, was not available as a consequence of hurricane damage. Two epochs of observations at 43 GHz are presented in this work to study the evolution of the millimeter-VLBI jet in total flux density through the radio outburst and obtain a high-resolution view of the inner-jet structure. The Brewster antenna could not be pointed and was excluded from the first of these observations (on 2017-11-10), thereby resulting in a significant loss of resolution particularly in the north-south direction (see Fig. 1). The latter observation, on 2018-05-04, was made with the full VLBA. Data were recorded at a data bit rate of 2048 Gb s^{-1}. See Table 1.

We reduced the data following standard procedures. A full discussion of all observational data including the polarization analysis and a multi-frequency analysis, and the discussion of the 86 GHz data that suffered severe gain and performance variations, will be presented elsewhere. In this work we focus on the imaging results at 43 GHz (λ7 mm) on November 10, 2017
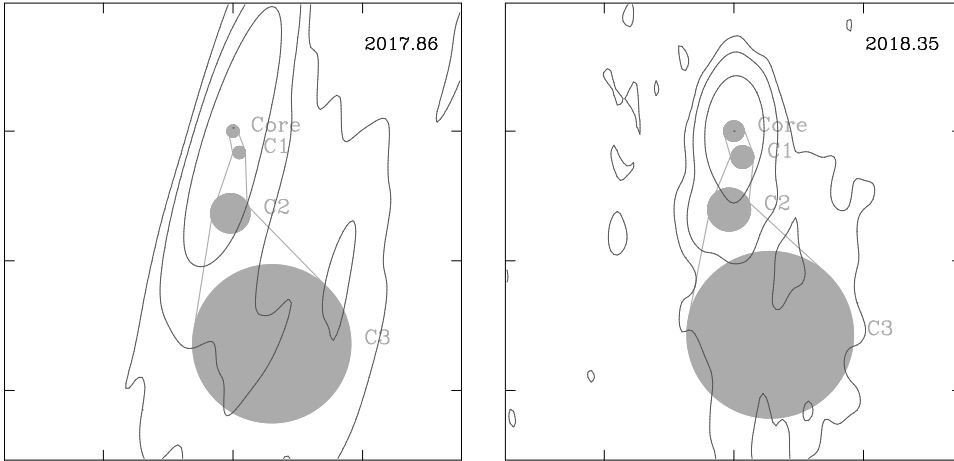
Fig. 2. Zoom into the 43 GHz VLBA images of TXS 0506+056 in Fig. 1, showing the Gaussian model functions fit to the interferometric visibilities and are presented in Table 2.
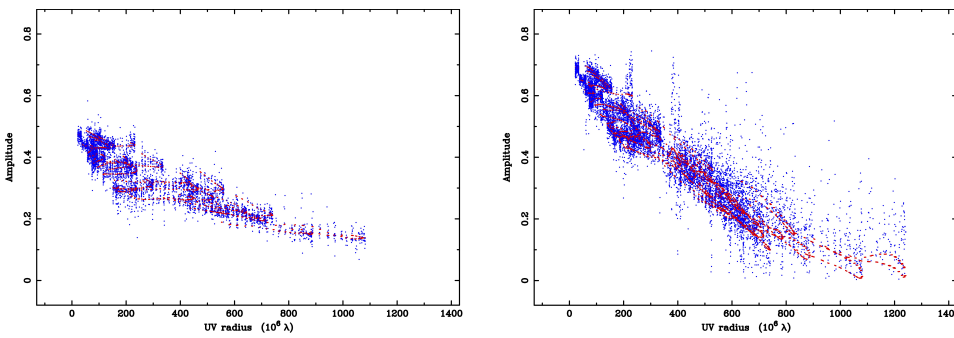

Fig. 3. Visibility amplitude (in Jy) as function of (u, v)-distance (in $G\lambda$) for Nov 11, 2017, and May 4, 2018. Data (averaged every 4 min for clarity) are shown in blue. The CLEAN model is shown in red. The data clearly show a brighter and less compact structure in May 2018.

and May 4, 2018, to study the evolution of the millimeter-VLBI jet in total flux density through the radio outburst in order to obtain a high-resolution view of the inner-jet structure.

3. Results

The $\lambda 7$ mm images presented in Fig. 1 show a core-jet structure pointing to the south, which is similar to but better resolved than the images of the MOJAVE survey at $\lambda 2$ cm. The image fidelity and particularly the angular resolution are different owing to the different observing conditions and array configurations. A close morphological inspection, however, shows no significant structural differences on scales larger than about 1 mas. On these scales, the jet does not show any clear isolated knots of locally enhanced brightness temperature for which speed measurements can be obtained. In particular, we can exclude the presence of a secondary jet core in the region roughly 1.2 mas southwest of the primary core, as suggested by Britzen et al. (2019), down to a limit of about 1 mJy; this would correspond to 5σ in our images.

The images of TXS 0506+056 show a compact core and a highly collimated inner jet within the inner parsec. The jet downstream shows a subsequently wider opening angle and the morphology is clearly limb brightened, reminiscent of the VLBI morphology found in several other teraelectronvolt blazars (e.g., Giroletti et al. 2004, 2008; Piner & Edwards 2014, 2018). We highlight the change in transverse structure from the inner parsec to the outer part of the jet by showing brightness profiles across the jet at two different locations (Fig. 1, right panels).

We fit the jet structure using Gaussian components (illustrated in Fig. 2). Variability of the source is detected on scales smaller than about 1 mas as illustrated in Fig. 3 (in which we plot visibility amplitude as a function of baseline length). The source gets brighter between November 2017 and May 2018, and the dominant emission region (the core) clearly expands, as

evidenced from the fall in the visibility function in the May 2018 epoch.

We modeled the interferometric visibilities to parametrize the source structure with Gaussian functions using the Levenberg–Marquardt algorithm implemented in the routine MODELFIT in the software DIFMAP (Sheperd 1997). The results of this modeling are shown in Table 2 and Fig. 2. A structure with four components aligned toward the south is consistently found in both observing epochs, and opens rapidly in size; compare the full width half maximum (FWHM) values in Cols. 6 and 13. We note that following Kovalev et al. (2005, see their Eq. (2)) the minimum resolvable size of a Gaussian component fitted to the visibilities would be of 21 μas and 12 μas for the first and the second epoch images, respectively, showing the robustness of our size estimates. We label these components Core (innermost, brightest component, in the millimeter regime often associated with a standing shock in the jet), as well as the jet features C1, C2, and C3. C1 represents a bright compact knot of emission that partially blends with the core and is located just (0.17–0.20) mas to the south. C2 and C3, in contrast, represent larger diffuse emission regions at about 0.6 mas and 1.7 mas south and south-southwest of the core, respectively. The most external region corresponding to C3 can also be modeled with two Gaussian functions at the jet edges, providing similar model statistics as presented for the single-component features. The apparent opening angle ϑ_{app} between adjacent components increases monotonically with increasing distance from the core: the inner jet between the core and C1 appears highly collimated[4] with an apparent opening angle of only $2°$ to $4°$; the

---

[4] We tested the residual visibilities when subtracting the core component in both epochs to confirm that the core is clearly resolved. In the case of the May 2018 epoch, this is immediately apparent from inspection of the overall visibility amplitudes as a function of baseline length (see Fig. 3).

Table 2. Gaussian model fitting results.

Date YYYY-MM-DD	ID	S [mJy]	$\Delta\alpha$ [μas]	$\Delta\delta$ [μas]	$FWHM$ [μas]	ϑ_{app} [°]	T_b [K]	Date YYYY-MM-DD	ID	S [mJy]	$\Delta\alpha$ [μas]	$\Delta\delta$ [μas]	$FWHM$ [μas]	ϑ_{app} [°]	T_b [K]
2017-11-10	Core	**275**	–	–	**68** [a]	–	5.3×10^{10}	2018-05-04	Core	**508**	–	–	**158** [a]	–	1.8×10^{10}
	C1	110	−49	−165	94	**4.3**	1.1×10^{10}		C1	91	−66	−200	175	**2.4**	2.6×10^{9}
	C2	85	20	−634	304	**12.7**	7.2×10^{8}		C2	77	37	−605	332	**10.7**	6.2×10^{8}
	C3	38	−299	−1640	1221	**23.5**	2.3×10^{7}		C3	54	−280	−1571	1286	**25.1**	2.9×10^{7}

Notes. S: total flux density; $\Delta\alpha$ and $\Delta\delta$: offsets in RA and DEC; FWHM: Gaussian FWHM, ϑ_{app}: apparent opening viewing angle w.r.t. previous feature; and T_b brightness temperature. In boldface, relevant values in the discussion. [a]Formal fit uncertainties are 1.1 μas and 0.2 μas, respectively.

angle between C1 and C2 is already substantially larger at 11° to 13°, whereas the outermost region between C2 and C3 has an apparent opening angle of 23° to 25°, which is compatible with the value of 28° determined at 15 GHz from stacked MOJAVE images in Pushkarev et al. (2017).

The flux density of the core changes between both epochs, almost doubling its value within six months while the other jet features do not show strong variability. Thus, we can attribute the radio outburst, seen at all radio frequencies, to a region inside the 7 mm VLBI core. Remarkably, the core size grows with time, so that the brightness temperature associated with it drops by a factor of three between the two epochs despite the rising flux density (compare Cols. 7 and 14). The outer rim of the core component moves by $(158 − 68)/2 = 45\,\mu$as (with a formal uncertainty smaller than 1 μas) within six months, which at a scale of 4.78 pc mas^{-1}, corresponds to a speed of about two times the speed of light. This effect of apparent superluminal expansion can be understood as a projection effect that occurs when relativistic plasma moves at a small angle to the line of sight, as is commonly observed for isolated jet knots in blazars (see, e.g., Cohen et al. 2007). Superluminal expansion in the core of the Seyfert galaxy III Zw 2 was reported in Brunthaler et al. (2000). An apparent superluminal core expansion is more unusual, in particular because the maximal speed of jet features in this object is below 1c (Lister et al. 2019).

4. Discussion

4.1. Structured jets as neutrino emitters

Bright neutrino emission is generally expected to be produced in flat-spectrum radio quasars (FSRQs) owing to the presence of a strong optical/UV seed photon field allowing interactions with high-energy protons inside the relativistic jet and subsequent pion production and decay (see, e.g., Murase et al. 2014). Lacking a strong broad-line region, BL Lacs, on the other hand, have been considered to be inefficient in neutrino production unless their jets carry an unexpectedly high power in accelerated protons (see Cerruti et al. 2019). In this context, the classification of TXS 0506+056 has created severe theoretical challenges for the neutrino emission models of this source. As a way out of this gridlock, it has been proposed that another external photon field may provide the seed photons for the photopion production. Popular variants of this approach are models that assume a spine-sheath structure of the jet with a highly relativistic inner spine and a slower mildly to non-relativistic outer sheath (Ghisellini et al. 2005). As a result of the strong velocity difference, the copious photons emitted in the slower sheath appear substantially boosted in the rest frame of the relativistic spine, so that enhanced photopion production can occur. Consequently, such a stratified jet is expected to be a much brighter neutrino source than a uniform (one-zone) jet (Tavecchio et al.

2014). At the same time, this model can solve the Doppler problem of the apparent contradiction of a low Doppler factor suggested by low apparent VLBI speeds of the jet and much higher Doppler factors implied by γ-ray observations of teraelectronvolt blazars (see, e.g., Blasi et al. 2013; Piner & Edwards 2018). Observational evidence for such a spine-sheath configuration of jets affected by the Doppler problem can in principle come from VLBI observations (e.g., Giroletti et al. 2004, 2008).

4.2. Increasing opening angle and superluminal core expansion

Both the increase of the apparent opening angle with distance and the rapid core expansion with time can be interpreted within two scenarios: first, the jet deceleration, as suggested by Georganopoulos & Kazanas (2003); and second, a spine-sheath structure of the jet, as suggested by Ghisellini et al. (2005). The inner jet between the core and C1 clearly appears to be highly collimated, which is suggestive of a fast relativistic flow. Beyond C1, the jet might decelerate and bend first to the east (C2) and then back southward (C3). This would be consistent with the model suggested by Georganopoulos & Kazanas (2003). Alternatively, the two components C2 and C3 might represent local brightness enhancements within a much wider diffuse jet. This second interpretation is consistent with the scenario put forward by Ghisellini et al. (2005).

The apparent superluminal expansion of the core can be interpreted as an adiabatic expansion of a highly relativistic plasma cloud traveling down the jet spine with an opening angle ϕ at an inclination angle ϑ to the line of sight. If we assume that $\vartheta < \phi$, the apparent core expansion would correspond to a component traveling down the jet with apparent $(28−57)c$ for a range of opening angles between 4° and 2°. In this case, we are looking into the jet and the external Compton emission (from a seed photon field originating in the sheath) dominates over the synchrotron self Compton (SSC) emission and the emission from hadronic processes. This is supported by the apparent opening angle of the inner jet between the core and component C1 of only (2−4)°. These values are fully consistent with the assumptions made in the modeling of the SED of TXS 0506+056 made by Ansoldi et al. (2018). Recently, Zhang et al. (2019) have presented a model, which explains both the 2014–2015 "neutrino flare" (IceCube Collaboration 2018b) and the detection of the single IceCube-170922A high-energy neutrino in 2017, by involving a persistent external photon field such as an outer jet sheath.

The expansion and deceleration of FRI jets at hundreds of parsecs to kiloparsecs (e.g., Laing & Bridle 2014) has been interpreted by several authors via collective interactions between jets and stellar winds, clouds, or even supernovae (Hubbard & Blackman 2006; Barkov et al. 2010; Bosch-Ramon et al. 2012; Perucho et al. 2014; Vieyro et al. 2019). The fast jet

expansion observed in TXS 0506+056 is reminiscent of such "geometrical flaring", although at parsec scales in this case ($r \leq 15$ pc to $r \sim 30$ pc for a viewing angle between 4° and 2°), which could be explained in terms of a single collision with a massive star (e.g., Hubbard & Blackman 2006). Evidence for such direct jet-star interactions has indeed been found, for example, by Müller et al. (2014). Interestingly, these scenarios naturally embed a population of protons in the jet, thus facilitating hadronic processes and neutrino production. These interactions are more probable toward the galactic nucleus, where the densities of stars and clouds are larger, and is precisely the region in which we observe the geometrical flaring to begin. Indeed, the mass loading from star-jet interactions in AGN has been considered a substantial contribution to the high-energy emission of blazars (De la Cita et al. 2019; Perucho et al. 2017; Torres-Albà & Bosch-Ramon 2019; Vieyro et al. 2019). In particular the SED and neutrino emission of TXS 0506+056 has also been interpreted and modeled in this context (Sahakyan 2018; Wang et al. 2018).

4.3. Discussion of other neutrino-source candidates

The FSRQ PKS 1424−418 has been associated with a petaelectronvolt neutrino with a chance coincidence of about 2σ (Kadler et al. 2016) based on the occurrence of a major radio outburst and a high-fluence kiloelectronvolt–gigaelectronvolt outburst coincident with the neutrino event IC35 in position and time. The Tracking Active Galactic Nuclei with Austral Milliarcsecond Interferometry (TANAMI) 8.6 GHz observations reveal a substantial brightening of the VLBI core on scales smaller than 1 mas. The high brightness temperature, flat radio spectrum, and rapid increase in flux density suggest a highly relativistic jet on these sub-milliarcsecond scales. In the context of our new finding regarding the spine-sheath structure of the TXS 0506+056 jet, it is interesting to note that the jet of PKS 1424−418 on scales of dozens of milliarcseconds has been found to be very diffuse and resolved, as pointed out by Ojha et al. (2010), and shows one of the widest opening angles in the whole TANAMI sample. This morphology is consistent with the morphology displayed by TXS 0506+056 as presented above. It should be noted, however, that several other VLBI jets have been observed to display similar wide-opening jet morphologies, yet these jets have not been associated with high-confidence neutrino events. A spine-sheath or geometrically flaring VLBI morphology alone is clearly not a sufficient condition to predict neutrino emission.

5. Summary and conclusions

We imaged the parsec-scale morphology of the jet in TXS 0506+056 at λ7 mm. The source shows a compact high brightness-temperature core and a highly collimated inner jet within the inner parsec from the core. Further downstream, the morphology changes into a subsequently limb-brightened jet with a wider opening.

We identified the location of the radio outburst associated with the IceCube-170922A neutrino event to within the core component, i.e., to linear deprojected scales smaller than 30 pc (unless the angle to the line of sight is much smaller than 2°).

The core expands with apparent superluminal velocity within eight months after the detection of the IceCube neutrino. This, along with the high brightness temperature of the core, suggests the presence of a highly relativistic beam on these scales.

The source morphology beyond 1 mas from the core is suggestive of a slower flow, either due to overall deceleration or jet-transversal velocity stratification. The slower flow can serve as a source of seed photons for photopion production and subsequent neutrino emission to explain the IceCube-170922A event as modeled, for example, by Ansoldi et al. (2018).

Further VLBI analysis of this source will include the study of the polarization properties and the spatially resolved milliarcsecond-scale continuum spectrum, but this is beyond the scope of the present publication.

References

Ansoldi, S., Antonelli, L. A., Arcaro, C., et al. 2018, ApJ, 863, L10
Barkov, M. V., Aharonian, F. A., & Bosch-Ramon, V. 2010, ApJ, 724, 1517
Blasi, M. G., Lico, R., Giroletti, M., et al. 2013, A&A, 559, A75
Bosch-Ramon, V., Perucho, M., & Barkov, M. V. 2012, A&A, 539, A69
Britzen, S., Fendt, C., Böttcher, M., et al. 2019, A&A, 630, A103
Brunthaler, A., Falcke, H., Bower, G. C., et al. 2000, A&A, 357, L45
Cerruti, M., Zech, A., Boisson, C., et al. 2019, MNRAS, 483, L12
Cohen, M. H., Lister, M. L., Homan, D. C., et al. 2007, ApJ, 658, 232
De la Cita, V. M., Bosch-Ramon, V., Paredes-Fortuny, X., Khangulyan, D., & Perucho, M. A&A, 591, A15
Georganopoulos, M., & Kazanas, D. 2003, ApJ, 594, L27
Ghisellini, G., Tavecchio, F., & Chiaberge, M. 2005, A&A, 432, 401
Giroletti, M., Giovannini, G., Feretti, L., et al. 2004, ApJ, 600, 127
Giroletti, M., Giovannini, G., Cotton, W. D., et al. 2008, A&A, 488, 905
Hubbard, A., & Blackman, E. G. 2006, MNRAS, 371, 1717
IceCube Collabaration (Aartsen, M. G., et al.) 2017, J. Instrum., 12, P03012
IceCube Collaboration, Fermi-LAT, MAGIC, et al. 2018a, Science, 361, 1378
IceCube Collaboration (Aartsen, M. G., et al.) 2018b, Science, 361, 147
Kadler, M., Krauß, F., Mannheim, K., et al. 2016, Nat. Phys., 12, 87
Kovalev, Y. Y., Kellermann, K. I., Lister, M. L., et al. 2005, AJ, 130, 2473
Kun, E., Biermann, P. L., & Gergely, L. 2018, MNRAS, 483, L42
Laing, R. A., & Bridle, A. H. 2014, MNRAS, 437, 3405
Lister, M. L., Aller, M. F., Aller, H. D., et al. 2009, AJ, 137, 3718
Lister, M. L., Aller, M. F., Aller, H. D., et al. 2018, ApJS, 234, 12
Lister, M. L., Homan, D. C., Hovatta, T., et al. 2019, ApJ, 874, 43
Müller, C., Kadler, M., Ojha, R., et al. 2014, A&A, 569, A115
Murase, K., Inoue, Y., & Dermer, C. D. 2014, Phys. Rev. D, 90, 023007
Ojha, R., Kadler, M., Böck, M., et al. 2010, A&A, 519, A45
Padovani, P., Oikonomou, F., Petropoulou, M., Giommi, P., & Resconi, E. 2019, MNRAS, 484, L104
Paiano, S., Falomo, R., Treves, A., & Scarpa, R. 2018, ApJ, 854, L32
Perucho, M., Martí, J. M., Laing, R. A., & Hardee, P. E. 2014, MNRAS, 441, 1488
Perucho, M., Bosch-Ramon, V., & Barkov, M. V. 2017, A&A, 606, A40
Piner, B. G., & Edwards, P. G. 2014, ApJ, 797, 25
Piner, B. G., & Edwards, P. G. 2018, ApJ, 853, 68
Pushkarev, A. B., Kovalev, Y. Y., Lister, M. L., & Savolainen, T. 2017, MNRAS, 468, 4992
Reimer, A., Böttcher, M., & Buson, S. 2019, ApJ, 881, 46
Richards, J. L., Max-Moerbeck, W., Pavlidou, V., et al. 2011, Ap&SS, 194, 2
Rodrigues, X., Gao, S., Fedynitch, A., Palladino, A., & Winter, W. 2019, ApJ, 874, L29
Righi, C., Tavecchio, F., & Guetta, D. 2017, A&A, 598, A36
Sahakyan, N. 2018, ApJ, 866, 109
Sheperd, M. C. 1997, ASP Conf. Ser., 125, 77
Tavecchio, F., Ghisellini, G., & Guetta, D. 2014, AJ, 793, L18
Torres-Albà, N., & Bosch-Ramon, V. 2019, A&A, 623, A91
Vieyro, F. L., Bosch-Ramon, V., & Torres-Albà, N. 2019, A&A, 622, A175
Wang, K., Liu, R. Y., Li, Z., Wang, X. Y., & Dai, Z. G. 2018, ArXiv e-prints [arXiv:1809.00601]
Zhang, B. T., Petropoulou, M., Murase, K., & Oikonomou, F. 2019, ArXiv e-prints [arXiv:1910.11464]